Articles

Physical Society of Indonesia

Journal of the Physical Society of Indonesia **2(2)**, 118-133 (2026)

https://doi.org/10.35895/jpsi.2.2.118-133.2026

Multi-Source Observational Analysis of Significant Weather Conditions Associated with the Structural Damage at Terminal 3 of Soekarno–Hatta International Airport on 6 April 2026

La Ode Ashamad Nusriah, Syahrajad Al Syarqiyah*

Meteorology Study Program, Sekolah Tinggi Meteorologi Klimatologi dan Geofisika, Tangerang 15221, Indonesia

(Received June 23, 2026; revised October 29, 2026; accepted October 31, 2026; published online November 01, 2026)

On April 6, 2026, intense rainfall (45.0 mm within one hour) coincided with ceiling failure at Gate 7, Terminal 3, Soekarno-Hatta International Airport, reported at 13:49 WIB (06:49 UTC). This study examines the associated weather using C-Band radar (CMAX), Himawari-9 imagery, Automatic Weather Station (AWS) records, ERA5 Low-Level Moisture Transport (LLMT), and radiosonde soundings. A compact convective system developed over the airport during 06:04–07:00 UTC, with radar reflectivity of 40–45 dBZ and cloud-top brightness temperatures of −62 to −69°C. AWS rainfall began at 06:10 UTC, peaked at 18.6 mm per 10 minutes at 06:30 UTC, and reached 45.0 mm by 06:50 UTC, accompanied by a 7.6°C temperature decrease and gusts up to 11.5 m s^{-1}. Cloud Convective Overlays (CCO) showed convective cloud growth south of the airport during 06:20–06:50 UTC. ERA5 LLMT at 925 and 825 hPa indicated enhanced moisture transport and a strong gradient near the airport, although its 0.25° resolution cannot resolve individual cells. The 00 UTC sounding showed weak CAPE (109 J kg^{-1}) and moderate KI (33.5); the 12 UTC sounding was post-event. Rainfall accompanied deep convection, but its causal role in ceiling failure remains unproven.

Keywords: *convective storm; extreme rainfall; weather radar; satellite observations; airport infrastructure*

This is an open access article under the CC BY-NC license.
Copyright © 2026 by Author. Published by Physical Society of Indonesia

1. INTRODUCTION

Significant weather represents a critical external factor affecting flight safety, particularly during the crucial phases of takeoff and landing, where extreme atmospheric conditions can trigger operational disruptions and potentially compromise airport infrastructure (Jarošová & Janošková, 2023). Weather phenomena such as thunderstorms, heavy rainfall, turbulence, wind shear, and microbursts are primary contributors to air traffic disturbances and can simultaneously exert direct pressure on terminal ceilings and drainage systems (Sasmito et al., 2020). High rainfall intensity also reduces horizontal visibility and can lead to water accumulation and flooding within terminal areas, further complicating airport operational management (Kim et al., 2023; Kwasiborska et al., 2023).

Although Convective Available Potential Energy (CAPE) values may be relatively low, ectreme rainfall can still occur in tropical regions when atmospheric moisture is high and Convective Inhibition (CIN) is not large enough to prevent convective initiation, reflecting characteristic features of tropical convective systems. This condition indicates that the occurrence of intense rainfall is not solely dependent on the available convective energy, but is also strongly influenced by the vertical distribution of atmospheric moisture and the upward mobility of air. Understanding this phenomenon is crucial in the airport context, as high-intensity rainfall, even under low CAPE conditions, can exert significant stress on ceilings, panels, and drainage systems, potentially resulting in structural damage and disruptions to airport operations (Taszarek et al., 2021; Syaifullah, 2017).

Extreme weather phenomena not only affect flight operations but also pose serious risks to airport infrastructure. Prolonged and intense precipitation can exert excessive pressure on drainage

*Contact Author: syahrajadal@gmail.com

systems, leading to water accumulation on rooftops, pooling in terminal areas, and water ingress onto ceiling panels and interior elements. These conditions can contribute to damage to terminal elements, which, if not promptly addressed, can produce a cascading effect across terminal sections, compromising passenger safety, comfort, and the continuity of airport operational activities (Liu et al., 2023; Gössling et al., 2023). Therefore, a comprehensive understanding of the meteorological conditions that accompany such events, together with a separate engineering assessment of the structural response, is essential, not only for short-term risk assessment but also for planning mitigation measures and enhancing future building designs.

The analysis of extreme weather events at modern airports cannot rely on a single type of observational data. Each instrument has limitations: radiosondes provide vertical atmospheric profiles but are only available at specific intervals, AWS measure local surface rainfall, satellite imagery depicts cloud distribution over large areas but is limited to cloud-top information, and radar provides rainfall reflectivity data yet is affected by range limitations and obstruction. Consequently, the integration of multi-source data is critical to thoroughly understanding atmospheric dynamics that produce extreme rainfall, affect terminal drainage and other infrastructure (Pauley & Ingleby, 2022). This approach also enables the identification of moisture patterns, precipitation intensity, and convective core locations most relevant to airport impacts.

Based on prior research and the inherent limitations of observational instruments, this study aims to characterize the meteorological conditions that coincided with the ceiling failure at Terminal 3 of Soekarno–Hatta International Airport, using multi-source observational data. The analyzed incident occurred on April 6, 2026, when intense rainfall and convective cloud activity affected the airport, the ceiling of the Gate 7 boarding lounge failed, and the weather also disrupted flight operations. This study documents the weather conditions; it does not assess the structural response of the building. This case study is especially important, as Soekarno–Hatta International Airport is one of Indonesia's busiest airports, and structural damage in the terminal area can significantly affect safety, security, and the smooth functioning of airport operations.

Several Indonesian case studies have combined radar, Himawari imagery, radiosonde stability indices, and ERA5 moisture transport to examine extreme rainfall (Hastuti & Mulsandi, 2017; Mulya, 2021; Saputra & Darmawan, 2025). A closely related study at Soekarno–Hatta Airport analyzed a flight-diversion case on 28 January 2025 using radiosonde, AWS, CCO, and radar data (Adzan et al., 2025). The present study differs from these in three respects. First, it relates the meteorological evidence to a documented damage incident at a major airport terminal rather than to a flight-diversion or flood event, and it adds ERA5 low-level moisture transport to the combination of datasets. Second, it places the radar, satellite, rain gauge, and reanalysis observations on a common 06:00–07:00 UTC timeline (Table 2) instead of discussing each dataset in isolation. Third, it states explicitly what each dataset can and cannot resolve for a compact convective cell, and lists the resulting limitations (Section 3.7)

2. METHOD

2.1 Study Area and Period

The study was conducted at Soekarno–Hatta International Airport, located at 6°07'12.4"S and 106°39'24.2"E. The investigated event was the structural damage at Terminal 3 of Soekarno–Hatta International Airport on 6 April 2026, which coincided with significant weather conditions occurring around the airport during the event. The analysis period covered 00:00 UTC on 6 April 2026 to 00:00 UTC on 7 April 2026. The geographical location of Soekarno–Hatta International Airport and its surrounding areas is presented in Figure 1.

Incident description. According to media reports based on statements by the airport operator, the ceiling of the Gate 7 boarding lounge (international departures) of Terminal 3 failed during heavy rain on Monday, 6 April 2026, releasing a large volume of water into the waiting area; the disturbance at this single roof point lasted about five minutes (Kompas.com, 2026a; Metro TV News, 2026). A widely shared video report placed the event at about 13:49 WIB (06:49 UTC) (Txt Transportasi Umum, 2026); no official time of failure was published. The operator attributed the damage to rainfall of high intensity accompanied by potential windshear (Suara.com, 2026) and stated that the rainwater discharge

exceeded the capacity of the drainage pipes (Kompas.com, 2026b). Repair of the area was targeted for completion on 8 April 2026. During the same period, 12 flights were diverted, 14 held, 13 made go-arounds, and one returned to the apron (Suara.com, 2026). No engineering assessment of the failure was available to the authors.

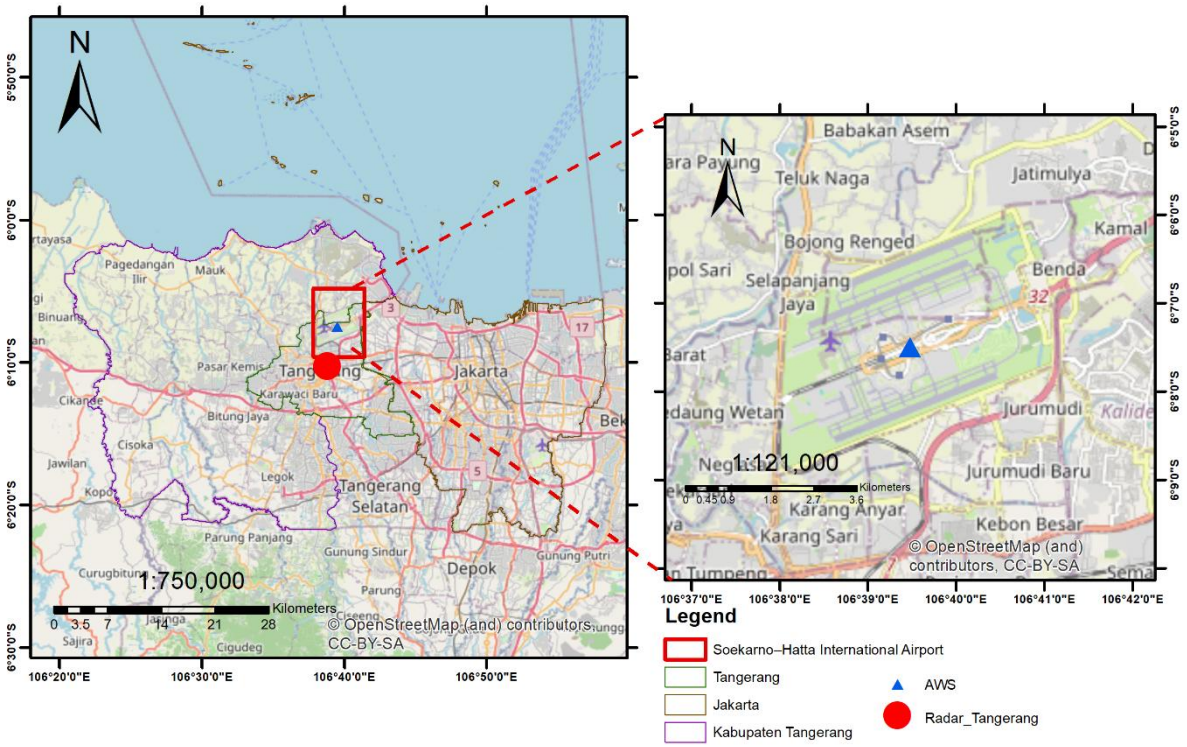


Figure 1. Research Study Area: Soekarno-Hatta International Airport and Surrounding Regions

2.2 Research Data

Five datasets were used in this study, as described in Sections 2.2.1–2.2.5: (1) C-Band weather radar, (2) Himawari-9 satellite imagery, (3) ERA5 reanalysis for low-level moisture transport, (4) Automatic Weather Station (AWS) rainfall observations, and (5) radiosonde upper-air soundings.

2.2.1 C-Band Weather Radar Data

Single-polarization C-Band weather radar data from the Class I Soekarno–Hatta Meteorological Station were utilized to identify maximum reflectivity values using the Column Maximum (CMAX) product, which displays the maximum reflectivity in each vertical column. Radar data were processed using Rainbow DART software. The CMAX images shown here are operational products used as provided; attenuation, calibration, beam blockage, and the cone of silence were not assessed in this study. CMAX has been reported to agree with surface rainfall observations from Automatic Weather Stations (AWS) and Automatic Rain Gauges (ARG) in previous studies (Tondang et al., 2023), but this agreement depends on the factors listed above.

2.2.2 Himawari-9 Satellite Data

Himawari-9 satellite data consisting of Band 8 (WV, 6.2 μm), Band 13 (IR1, 10.4 μm), and Band 15 (IR2, 12.4 μm) were obtained in NetCDF format. These data were used to identify the spatial distribution of cumulonimbus (Cb) clouds using the Cloud Convective Overlays (CCO) method implemented in Python. The CCO method employs the Split Window and Dual Channel Difference algorithms. Himawari-9 carries the same Advanced Himawari Imager design and band configuration as Himawari-8, so the thresholds published for Himawari-8 were applied without modification; their sensitivity was not tested (Section 3.7).

$$T_{IR1} - T_{IR2} \leq 2\,K \quad \text{and} \quad T_{IR1} - T_{WV} \leq 3\,K \tag{1}$$

In Equation (1), TWV, TIR1, and TIR2 are the brightness temperatures (in K) of Band 8 (WV, 6.2 μm), Band 13 (IR1, 10.4 μm), and Band 15 (IR2, 12.4 μm), respectively. A pixel is classified as Cb only when both conditions are satisfied simultaneously (an overlay of the two conditions, i.e., logical AND). The first condition is the split-window test and the second is the dual-channel (water vapor minus infrared) difference test. A small IR1–IR2 difference indicates an optically thick, cold cloud top, whereas thin cirrus gives larger differences; an IR1–WV difference of only a few kelvin indicates a cloud top near the tropopause, where the water-vapor and window-channel brightness temperatures converge, as in deep convection (Hastuti & Mulsandi, 2017; Mulya, 2021). The CCO technique is effective for detecting convective cloud systems associated with heavy rainfall and severe weather events (Syaifullah & Nuryanto, 2016; Hastuti & Mulsandi, 2017; Mulya, 2021).

2.2.3 ERA5 Reanalysis Data for Low-Level Moisture Transport (LLMT)

ERA5 hourly reanalysis data on pressure levels from the European Centre for Medium-Range Weather Forecasts (ECMWF) were utilized at a horizontal resolution of 0.25° × 0.25° (approximately 28 km). The variables included zonal wind (u), meridional wind (v), and specific humidity (q) at the 925 hPa and 825 hPa levels. The data were processed using the Grid Analysis and Display System (GrADS) to generate hourly Low-Level Moisture Transport (LLMT) maps, computed as the magnitude of the horizontal moisture flux, $LLMT = q\cdot\sqrt{(u^2 + v^2)}$, in g kg^{-1} m s^{-1}. ERA5 provides a globally consistent atmospheric reanalysis dataset with high temporal and spatial resolution and has been widely applied in meteorological and climatological studies (Hersbach et al., 2020). LLMT represents the transport of atmospheric moisture within the lower troposphere and is used as an indicator of the low-level moisture environment favorable to convective development (Saputra & Darmawan, 2025). Because of its resolution, ERA5 describes the mesoscale moisture environment and cannot resolve individual convective cells a few kilometers across.

2.2.4 Automatic Weather Station (AWS) Data

Rainfall observations were obtained from the AWS Digi Stamet Cengkareng (station ID STA5082; 6.125° S, 106.658° E), operated by the Soekarno–Hatta Class I Meteorological Station and located about 0.6 km from the study-area reference point defined in Section 2.1. The station reports at 10-minute intervals. Rainfall is reported as the cumulative amount since 00:00 UTC, reset daily; the smallest increment in the record is 0.2 mm, taken here as the gauge resolution. The rainfall flag field is empty for all records in the file used. Ten-minute amounts were obtained by differencing successive cumulative values, and 60-minute accumulations as the running sum of six consecutive 10-minute amounts. Timestamps are taken to mark the end of each 10-minute interval. Rain gauges can under-catch at high rainfall intensities, so the values reported here may slightly underestimate the actual rainfall.

2.2.5 Upper-Air Observation (Radiosonde) Data

Radiosonde observations from the Class I Soekarno–Hatta Meteorological Station were processed using Rawinsonde Observation (RAOB) software to produce upper-air sounding profiles. These data were used to evaluate atmospheric stability indices, vertical wind profiles, and thermodynamic conditions associated with significant weather during the event. Radiosonde observations provide detailed vertical information on atmospheric structure and remain the primary source for atmospheric sounding and severe weather analysis (Syaifullah, 2017).

2.3 Data Analysis

2.3.1 Radar Reflectivity Analysis (CMAX)

C-Band radar data were processed using Rainbow DART to generate CMAX products and identify maximum reflectivity values during periods of very heavy rainfall on 6 April 2026. The use of CMAX enables the representation of maximum reflectivity throughout the atmospheric column and has been compared with surface rainfall in previous studies (Tondang et al., 2023).

2.3.2 Cumulonimbus Cloud Distribution Analysis (CCO)

Multi-channel Himawari-9 imagery (Bands 8, 13, and 15) was processed using Python and the Cloud Convective Overlays (CCO) method to examine the spatial and temporal distribution of cumulonimbus clouds over Soekarno–Hatta Airport and surrounding areas during the event (Syaifullah & Nuryanto, 2016; Hastuti & Mulsandi, 2017; Mulya, 2021).

2.3.3 Low-Level Moisture Transport (LLMT) Analysis

ERA5 data were processed using GrADS to generate hourly LLMT maps at the 925 hPa and 825 hPa levels for 06:00 and 07:00 UTC on 6 April 2026. Enhanced LLMT values indicate stronger moisture transport and a moister low-level environment that supplies water vapor for convective development and precipitation formation; convergence of this flux was not computed in this study (Saputra & Darmawan, 2025).

2.3.4 Rainfall Analysis (AWS)

AWS rainfall observations were processed using Python to derive 10-minute rainfall amounts (by differencing the cumulative values) and a 60-minute running accumulation throughout the study period. The resulting rainfall characteristics were used to assess precipitation intensity and temporal variability during the event (Sokol et al., 2021).

2.3.5 Atmospheric Stability Analysis (Radiosonde)

Radiosonde data were processed using RAOB software and interpreted using atmospheric stability indices, including CAPE, CIN, K Index (KI), Showalter Index (SI), and SWEAT Index, following the classification criteria presented in Table 1 (Fibriantika & Mayangwulan, 2020; Kusumawardani & Azani, 2022; Syaifullah, 2017). RAOB reports CIN as a negative value, so the CIN thresholds in Table 1 are applied to its magnitude (for example, −128 J kg^{-1} corresponds to a magnitude of 128 J kg^{-1}). The thresholds are empirical classes used in Indonesian operational and research studies rather than universal physical limits, and are used here only to describe the soundings qualitatively. SWEAT is available only for the 00 UTC sounding and is therefore not used to compare the two soundings.

Table 1 Classification of Atmospheric Stability Indices

Stability Index	Weak	Moderate	Strong
CAPE (J kg^{-1})	< 1000	1000–2500	> 2500
CIN (J kg^{-1})	< 50	51–199	≥ 200
K Index (KI)	< 29	29–37	> 37
Showalter Index (SI)	> 4	4 to −4	< −4
SWEAT Index	< 135	135–239	> 239

Source: (Fibriantika & Mayangwulan, 2020; Kusumawardani & Azani, 2022; Syaifullah, 2017).

3. RESULTS AND DISCUSSION

3.1 Radar Reflectivity Analysis (CMAX)

Figure 2 presents the temporal sequence of C-Band weather radar CMAX (Column Maximum) reflectivity products from the Soekarno-Hatta Class I Meteorological Station, recorded at 06:04, 06:20, 06:36, and 07:00 UTC on April 6, 2026. The CMAX product displays the maximum reflectivity value throughout the entire atmospheric column at each grid point, showing the spatial distribution and relative intensity of radar echoes across the radar coverage area (Tondang et al., 2023).

At 06:04 UTC, a compact convective cell was identified directly over the airport, with maximum reflectivity reaching approximately 42 dBZ, indicating a moderate-to-strong radar echo (the relation between reflectivity and surface rainfall depends on the drop-size distribution and the radar sampling

height, so the echo is not converted into a rainfall intensity here). The convective core was surrounded by a broader area of lower reflectivity, suggesting active convective development over the airport vicinity. By 06:20 UTC, the cell intensified slightly, with maximum reflectivity increasing to 45 dBZ and the moderate reflectivity region expanding laterally. This evolution was consistent with the occurrence of heavy surface rainfall, with the AWS recording 9.0 mm in the 10-minute interval at 06:20 UTC and a 45.0 mm event total by 06:50 UTC (Section 3.4). At 06:36 UTC, the convective core weakened marginally, with maximum reflectivity decreasing to 40 dBZ, while the surrounding precipitation area spread toward the Java Sea coast, indicating a transition from the mature stage toward the dissipation phase. By 07:00 UTC, reflectivity increased again to approximately 44 dBZ, accompanied by the development of two distinct convective cells to the northwest and west of the airport. This pattern suggests multicellular convective redevelopment, although the cause of this redevelopment cannot be determined from the data analyzed here.

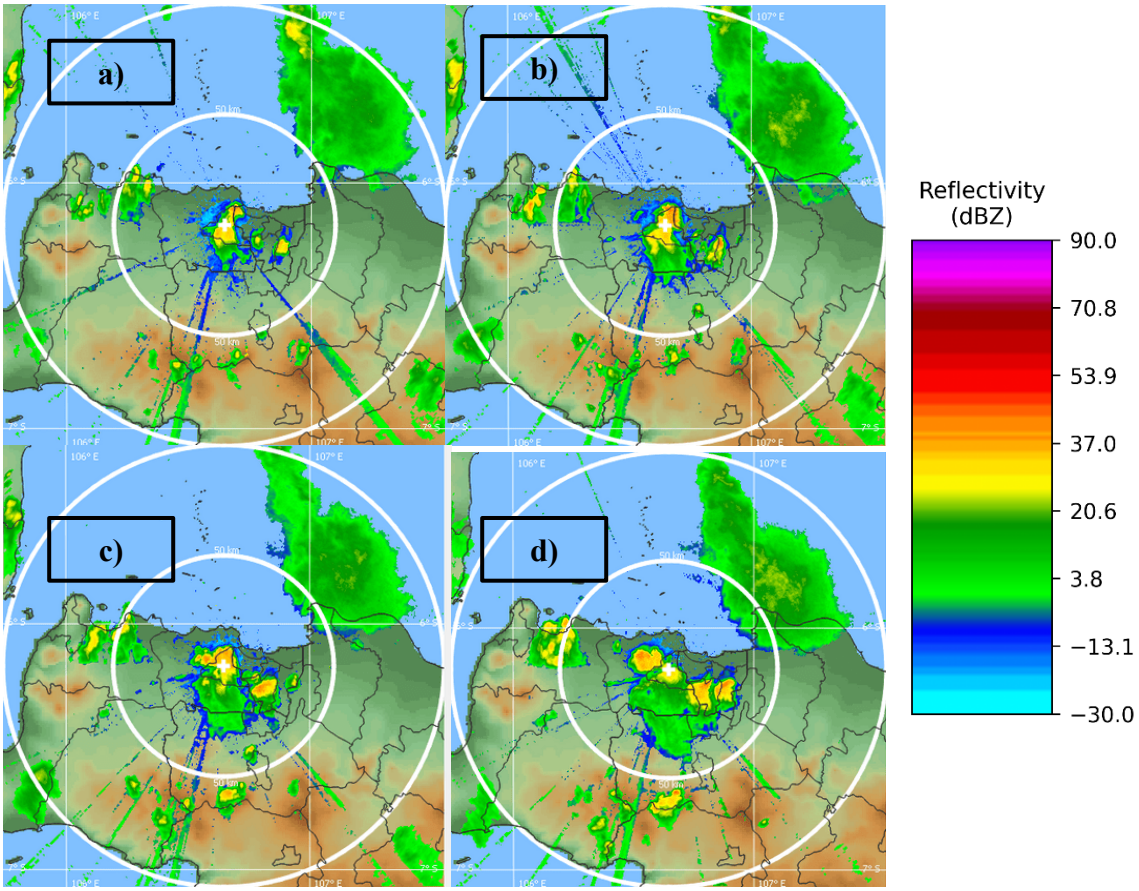


Figure 2. Evolution of CMAX Radar Reflectivity over CGK Airport: (a) 06:04, (b) 06:20, (c) 06:36, and (d) 07:00 UTC on April 06, 2026

These findings are consistent with the convective evolution described by Paski et al. (2020), although the maximum reflectivity observed in this study (40–45 dBZ) was lower than the 60–65 dBZ reported within intense cumulonimbus cores. Possible reasons are attenuation at C-band in heavy rain, beam geometry, calibration, and sampling close to the radar site (cone of silence), none of which was assessed here. The four images (06:04, 06:20, 06:36, and 07:00 UTC) are also unevenly spaced and do not sample the 06:20–06:40 UTC window in which the AWS recorded its maximum rainfall, so the maxima shown may underestimate the peak. Converting reflectivity with the Marshall–Palmer relation ($Z = 200R^{1.6}$) gives about 12 mm h^{-1} at 40 dBZ and 24 mm h^{-1} at 45 dBZ, which is about half of the 60-minute AWS amount (45.0 mm) and about one fifth of the peak 10-minute AWS rate (about 112 mm h^{-1}). CMAX is therefore used in this study only qualitatively, as an indicator of the timing and evolution

of the convective cell, and not as a quantitative estimate of rainfall intensity; no radar–gauge comparison was performed.

3.2 Himawari-9 Band 13 (IR1) Brightness Temperature Distribution

Figure 3 presents the temporal evolution of Himawari-9 Band 13 (IR1, 10.4 μm) brightness temperature (BT) over Soekarno-Hatta International Airport and surrounding areas from 05:40 to 07:00 UTC on April 6, 2026. In the color scale, dark blue to black indicates warm surfaces or low clouds (BT of about +14 to +60°C), green to olive indicates BT of about −13 to −41°C, orange indicates about −48 to −62°C, and peach to pink indicates very cold cloud tops (about −62 to −80°C), indicative of deep convective cloud systems. The airport is located at about 6.12°S, 106.66°E.

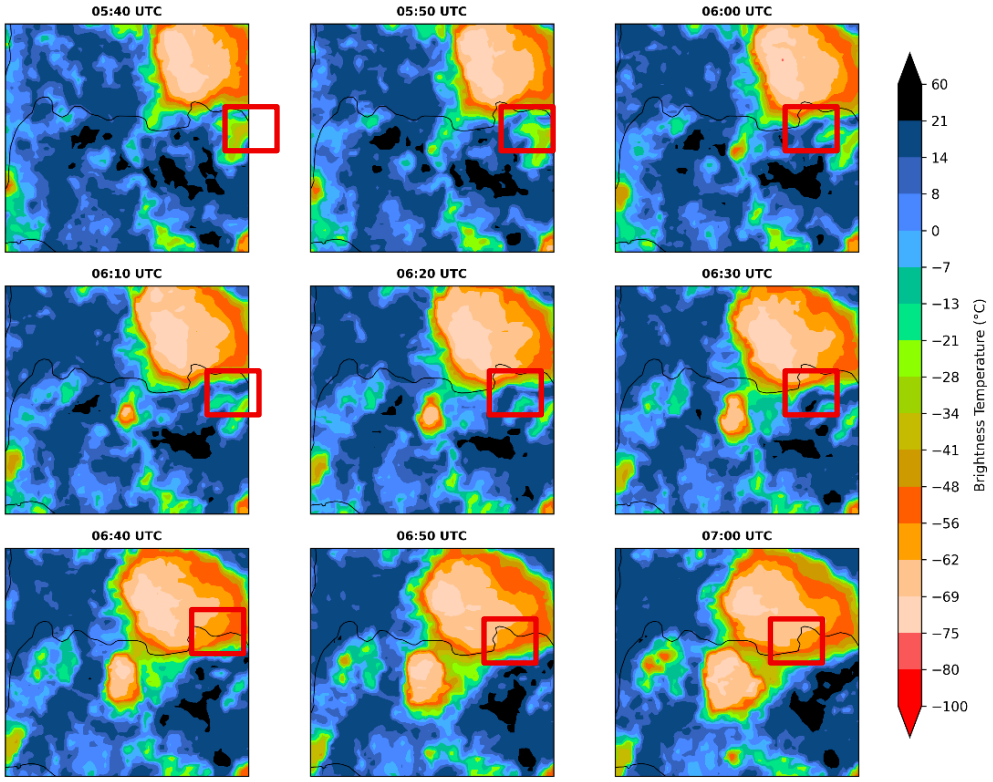


Figure 3. Himawari-9 Band 13 (IR1) Brightness Temperature Distribution over Soekarno-Hatta International Airport. The airport is located at about 6.12°S, 106.66°E. BT in °C. The red boxes mark the airport location. All panels show the same domain; the coastline is shown for geographic reference.

At 05:40 UTC, a broad shield of cold cloud tops (orange to peach, BT of about −48 to −69°C) was already present in the north-northeast of the domain, consistent with organized convection over the Java Sea, and it persisted through 07:00 UTC. The land area around and south of the airport was largely warm (blue to black, BT above 0°C) from 05:40 to 06:00 UTC, with only scattered green patches (BT of about −13 to −34°C), indicating no deep convection there yet. At 06:10 UTC, a small compact cluster with orange colors (BT of about −48 to −56°C) appeared over land south of the coastline. From 06:20 to 06:30 UTC, this cluster intensified, with BT of about −56 to −62°C, corresponding to the period of most intense precipitation in the AWS record and to the radar maximum in the CMAX product (Figure 2). By 06:40 UTC, its core reached about −62 to −69°C (peach) and covered a larger area, consistent with the maturation and lateral expansion of the cumulonimbus anvil, and at 06:50 and 07:00 UTC it remained large with some expansion and peripheral changes. The observed BT evolution is consistent with Nisa et al. (2022), who reported cumulonimbus cloud top temperatures reaching -67 to -78°C during peak convective phases over Kalimantan.

3.3 Cloud Convective Overlays (CCO) Detection

The CCO detection analysis using Himawari-9 multi-channel data (Bands 8, 13, and 15) is presented in Figure 4, showing the spatial distribution of convective (Cb, red) and non-convective (Non-Cb, light blue) cloud objects over Jakarta and surrounding areas from 06:10 to 07:00 UTC on April 6, 2026. The CCO method employs the Split Window and Dual Channel Difference algorithms, applying the two conditions of Equation (1) for Cb cloud identification (Hastuti & Mulsandi, 2017; Mulya, 2021).



Figure 4. Cloud Convective Overlays (CCO) Detection of Convective (Cb) and Non-Convective (Non-Cb) Cloud Objects over Soekarno-Hatta International Airport and Surrounding Areas, 06:10–07:00 UTC on April 6, 2026. The airport is located at about 6.12°S, 106.66°E (red boxes). All panels show the same domain; the coastline is shown for geographic reference.

At 06:10 UTC, Cb cloud objects were predominantly detected in the northern corner of the domain, consistent with the existing organized convection over the Java Sea identified in the BT analysis (Figure 3). Only minor isolated Cb pixels were detected within the land domain south of the airport at this time. By 06:20 UTC, a small but distinct Cb cluster appeared in the southern portion of the land domain, marking the initiation of convective cloud development directly south of the airport. This cluster grew notably at 06:30 UTC, expanding in spatial extent and intensity, consistent with the rapid deepening of the convective core identified in both the BT analysis (Figure 3) and the CMAX product (Figure 2). The most significant development was observed from 06:40 to 06:50 UTC, where the Cb cluster reached its largest and most cohesive extent, with a compact, rounded Cb object reflecting the presence of a mature convective core. At 07:00 UTC, the Cb cluster remained large but showed structural modification at the periphery, consistent with the multicellular convective redevelopment observed in the radar analysis (Figure 2).

The CCO cluster first appears south of the airport at 06:20 UTC, whereas the radar shows a 42 dBZ cell directly over the airport already at 06:04 UTC, and the largest Cb object (06:40–06:50 UTC) occurs while radar reflectivity is decreasing (40 dBZ at 06:36 UTC). Several factors can explain this offset in space and time without implying that the datasets disagree. First, parallax: at the airport location Himawari-9 views the surface at a zenith angle of about 40°, so a cloud top at 14–16 km is displaced by roughly 12 km away from the sub-satellite point (toward the west-southwest) relative to its true position; parallax was not corrected here, so the cluster south of the airport in Figs. 3 and 4 may lie closer to the airport than it appears. Second, the nominal image time is the start of the 10-minute full-disk scan, and the Indonesian sector is scanned several minutes later, so the actual observation time can differ from the

nominal time. Third, cloud-top cooling lags the onset of precipitation, and the anvil persists after radar reflectivity peaks, so the largest CCO object need not coincide with the radar maximum. The agreement among Figs. 2–4 should therefore be read as qualitative consistency of the 06:00–07:00 UTC convective evolution, not as a point-to-point match.

These findings align with Hastuti and Mulsandi (2017), who demonstrated that the CCO method effectively identifies cumulonimbus clouds associated with extreme rainfall events over Indonesia. Syaifullah and Nuryanto (2016) similarly validated the capability of this technique to detect convective cloud systems producing heavy rainfall in the Indonesian Maritime Continent. The temporal evolution of CCO-detected Cb objects in this study is in qualitative agreement with both the BT distribution (Figure3) and the CMAX radar reflectivity analysis (Figure 2), providing qualitative multi-source evidence consistent with a convective cloud system as the source of the heavy rainfall at Soekarno-Hatta International Airport.

3.4 Rainfall Analysis (AWS)

Figure 5 shows the rainfall recorded at the AWS Digi Stamet Cengkareng (Section 2.2.4) on 6 April 2026 as 10-minute amounts (bars) and as a 60-minute running accumulation (line). The record shows a highly concentrated precipitation event: the first rainfall (0.6 mm) was recorded in the interval ending at 06:10 UTC and was essentially over by 06:50 UTC, after which only 0.2 mm was recorded (at 07:20 UTC).

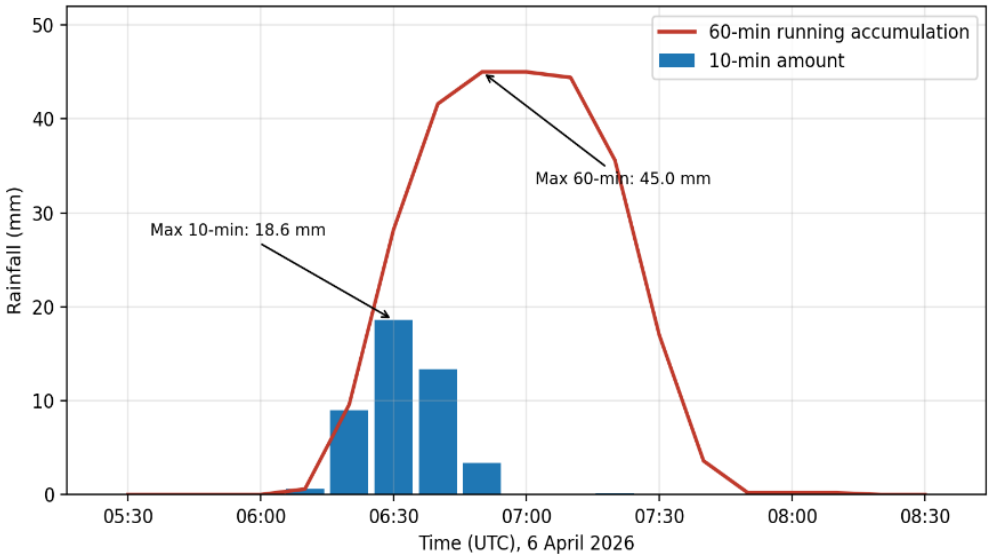


Figure 5. Rainfall at AWS Digi Stamet Cengkareng on April 6, 2026: 10-minute amounts (bars) and 60-minute running accumulation (line)

The 10-minute amounts increased from 0.6 mm at 06:10 UTC to 9.0 mm at 06:20, 18.6 mm at 06:30, and 13.4 mm at 06:40, then fell to 3.4 mm at 06:50 UTC. The maximum 10-minute amount of 18.6 mm is equivalent to an intensity of about 112 mm h^{-1}. The 60-minute running accumulation reached its maximum of 45.0 mm by 06:50 UTC, so the whole event total fell within about 40 minutes; the daily total for 6 April was 45.2 mm. Because the 60-minute value is a running sum, it peaks after the time of maximum intensity; the period of maximum rainfall intensity is therefore 06:20–06:40 UTC, which coincides with the radar maximum (06:20 UTC) and with the cloud top cooling toward its coldest class (about −62 to −69°C at 06:40 UTC), whereas the largest CCO cluster (06:40–06:50 UTC) coincides with the decay of rainfall at the station (Table 2). With 45.0 mm in 60 minutes, the event exceeds the 20 mm h^{-1} threshold that BMKG uses for heavy rainfall (BMKG, 2010) by more than a factor of two. The daily total (45.2 mm), however, is below the BMKG daily criterion for heavy rain (50 mm per day) and far below the extreme category (> 150 mm per day); the term “extreme rainfall” is therefore used in this paper in a descriptive sense for the unusual short-duration intensity, not as a formal BMKG category. A climatological assessment of how unusual this intensity is at Soekarno–Hatta (for example, a return

period) was not possible with the AWS data available here and should be addressed in future work. The onset of the AWS signal is in qualitative agreement with the radar (Figure 2) and Himawari-9 (Figure 3) evolution, although the datasets differ in sampling interval and were not co-located. Rain gauges can under-catch at high intensities, so these amounts may be slightly underestimated.

The AWS surface variables also show a convective signature. Between 05:40 and 06:40 UTC the air temperature fell from 31.9°C to 24.3°C, relative humidity rose from about 62% to 89%, and the station pressure rose transiently by about 1.1 hPa at 06:20 UTC. The 10-minute mean wind speed increased from 1–2 m s^{-1} before 06:00 UTC to 5.9 m s^{-1} at 06:20 and 7.7 m s^{-1} at 06:40 UTC, with maximum gusts of 8.8 m s^{-1} at 06:20 and 11.5 m s^{-1} (about 22 kt) at 06:40 UTC, and the wind direction varied between 194° and 329° during 06:20–06:40 UTC. This combination is consistent with a convective downdraft and cold-pool outflow. The recorded gusts are moderate, so wind loading at the station does not appear extreme; however, a single station cannot exclude stronger local gusts, and the potential windshear mentioned by the airport operator could not be evaluated here because no Doppler wind or low-level windshear data were analyzed.

The temporal pattern of precipitation, characterized by a rapid onset, a sharp and narrow peak, and an abrupt cessation, is highly characteristic of convective rainfall produced by an isolated or quasi-stationary cumulonimbus system. This pattern is consistent with findings reported by Lubis et al. (2022) in their analysis of record-breaking precipitation in Jakarta in January 2020, which highlighted the role of organized mesoscale convective systems in producing extreme short-duration rainfall events over the Jakarta region. Furthermore, Lubis and Respati (2021) noted that extreme rainfall events over Java are frequently characterized by short-duration high-intensity pulses driven by synoptic-scale moisture flux convergence and equatorial wave activity. A rainfall total of 45.0 mm in approximately one hour represents a substantial hydrological input to drainage systems; whether it exceeded their design capacity, or contributed to the failure, cannot be determined without drainage and engineering data. The reported failure time (about 06:49 UTC, Section 2.1) falls at the end of the 40-minute rainfall burst, when 41.6 mm had accumulated at the AWS by 06:40 UTC and 45.0 mm by 06:50 UTC, which is consistent with the operator's statement that the water discharge exceeded the capacity of the drainage pipes (Kompas.com, 2026b). Because AWS timestamps mark the end of each 10-minute interval, the failure at about 06:49 UTC fell within the interval ending at 06:50 UTC (3.4 mm), about 20 minutes after the interval of peak rainfall (ending at 06:30 UTC). However, the failure time is taken from a social-media report, no official failure time or engineering assessment was available to the authors, and the structural response was not analyzed. The rainfall is therefore treated as a coinciding and plausible contributing condition, not as a demonstrated cause.

3.5 Low-Level Moisture Transport (LLMT) Analysis

The Low-Level Moisture Transport (LLMT) derived from ERA5 reanalysis data at 925 hPa and 825 hPa pressure levels is presented in Figure 6, showing conditions at 06:00 and 07:00 UTC on April 6, 2026. LLMT quantifies the horizontal transport of atmospheric moisture in the lower troposphere and serves as an indicator of the low-level moisture supply available for convective development (Saputra & Darmawan, 2025). Note that LLMT is a moisture flux magnitude and is not itself a measure of convergence; convergence is inferred here only qualitatively from horizontal gradients in the LLMT field. The moisture-flux divergence, $-\nabla\cdot(qV)$, was not calculated in this study; therefore no statement is made about the presence or location of a convergence zone, and the gradient is described only as a feature of the transport field.

At 925 hPa and 06:00 UTC, the highest LLMT values (deep red, > 41.55 g kg^{-1} m s^{-1}) were located over western Java (Banten), west-southwest of the airport, with a secondary maximum over the western Java Sea in the north-western corner of the domain. An area of suppressed moisture transport (deep blue, < 5.19 g kg^{-1} m s^{-1}) lay over the Java Sea to the north-east and east, so that the airport was located within a strong horizontal LLMT gradient between these regions. Such a gradient is consistent with, but does not by itself demonstrate, low-level moisture flux convergence near the airport. At 825 hPa and 06:00 UTC, high LLMT values covered most of the northern and western parts of the domain, including the Jakarta area, whereas a minimum was located over southern West Java. At 07:00 UTC, the 925 hPa maximum remained over western Java, west-southwest of the airport, while the area of high

LLMT over the western Java Sea weakened; the airport remained on the eastern flank of the high-LLMT region. At 825 hPa the pattern was similar to that at 06:00 UTC. Because the 06:00 and 07:00 UTC fields coincide with the event, they may partly reflect the convection itself (for example, outflow-modified low-level winds and moisture) rather than the pre-storm environment.

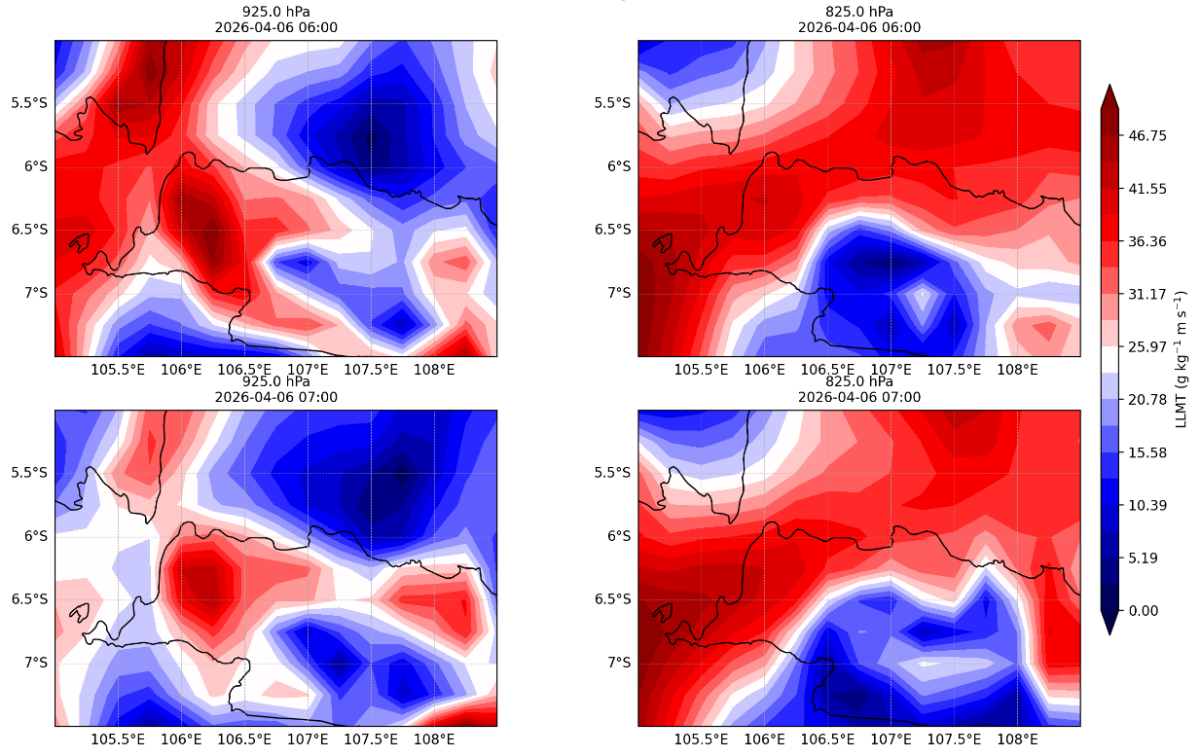


Figure 6. Low-Level Moisture Transport (LLMT) at 925 hPa and 825 hPa Levels on April 6, 2026 (06:00 and 07:00 UTC)

The presence of enhanced low-level moisture over western Java and the western Java Sea during the event is consistent with the role of low-level moisture flux convergence reported by Lubis et al. (2022), who linked the record-breaking Jakarta precipitation of January 2020 to northerly surges and equatorial waves with enhanced low-level moisture flux convergence, and with the use of low-level moisture transport as an indicator of convective potential by Saputra and Darmawan (2025). In the present case, however, the high-LLMT axis lay over western Java and the western Java Sea rather than forming a clear transport pathway from the Java Sea toward the airport, and ERA5 at 0.25° (about 28 km) cannot resolve a convective cell a few kilometers across. The LLMT analysis therefore suggests a moist low-level environment around the airport at the mesoscale, but does not identify the trigger of the individual convective cell.

3.6 Atmospheric Stability Analysis Based on Radiosonde Data (Skew-T Log-P)

Analysis of upper-air data from the Soekarno-Hatta Class I Meteorological Station provided thermodynamic profiles at 00 UTC (about six hours before the rainfall) and at 12 UTC (about five hours after the rainfall ended) on April 6, 2026. The Skew-T Log-P diagrams for both observation times are presented in Figure 7a (00 UTC) and Figure 7b (12 UTC), respectively.

At 00 UTC (Figure 7a), the atmosphere exhibited a relatively weak convective environment. CAPE was 109 J kg^{-1} (weak category), CIN −128 J kg^{-1} (magnitude 128 J kg^{-1}, moderate category), K Index (KI) 33.5 (moderate), Showalter Index (SI) 1.4 (moderate), and SWEAT Index 204 (moderate). The LCL was 233 m AGL and the LFC 3043 m AGL, and a shallow radiation inversion was present at 132 m AGL. The 12 UTC sounding (Figure 7b) was launched about five hours after the rainfall ended and therefore describes a post-event environment that may already have been modified by storm outflow and evening cooling. It showed CAPE of 638 J kg^{-1}, CIN −168 J kg^{-1}, DCAPE (6.0 km) of 603 J kg^{-1}, KI of 35.4 (moderate), and SI of −0.5. CAPE and CIN are the values output by the RAOB software; the

lifted parcel used by the software was not varied in this study. These 12 UTC values are reported for completeness and are not used to infer the pre-convective environment, the storm character, or the vertical-velocity potential.

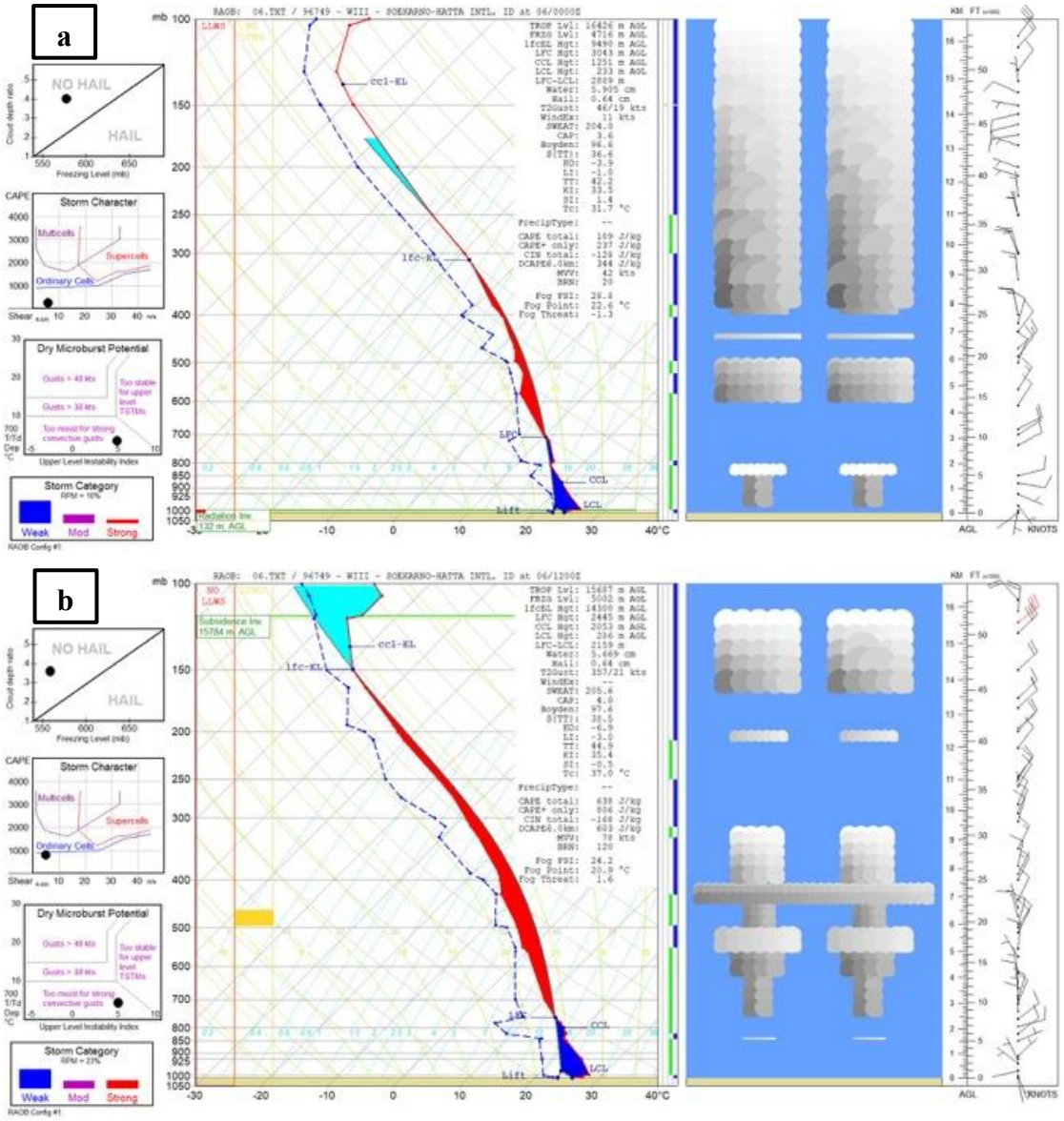


Figure 7. Atmospheric Sounding Profiles at Soekarno-Hatta International Airport on April 06, 2026: (a) 00:00 UTC and (b) 12:00 UTC

These findings are consistent with Taszarek et al. (2021), who noted that in tropical environments heavy rainfall can occur even under relatively low CAPE regimes when atmospheric moisture content is high and CIN is moderate, and with the low-CAPE framing in the Introduction. Fibriantika and Mayangwulan (2020) and Syaifullah (2017) further noted that in Indonesia moderate KI values in the range of 29 to 37 are frequently associated with convective rainfall events, particularly when low-level moisture transport is enhanced; the KI of 33.5 at 00 UTC falls within this range. Because the 12 UTC sounding was launched about five hours after the rainfall ended, its higher CAPE and KI cannot be taken as evidence of pre-storm intensification, and no conclusion is drawn about a transition in storm character or about outflow near the tropopause. A sounding closer to the event time (for example, a special 06 UTC launch or a model-derived profile) would be needed to characterize the pre-convective environment.

3.7 Synthesis and Limitations

Table 2 places the observations of each dataset on a common timeline. The radar echo over the airport, the cold cloud tops, the growth of the CCO cluster south of the airport, and the AWS rainfall signal all fall within the same 06:00–07:00 UTC window, and the sequence is physically coherent. Taken separately, the highest radar reflectivity among the four available images (45 dBZ) was observed at 06:20 UTC, the coldest cloud-top class in the brightness-temperature images (about −62 to −69°C) at 06:40 UTC, the peak AWS 10-minute rainfall (18.6 mm) in the interval ending at 06:30 UTC, and the largest CCO object at 06:40–06:50 UTC. These times differ by up to about 20 minutes, which is consistent with the sampling differences discussed in Section 3.3 (unevenly spaced radar images with none between 06:20 and 06:36 UTC, 10-minute satellite and AWS intervals, and parallax). The ERA5 fields (06:00 and 07:00 UTC) and the radiosonde soundings (00 and 12 UTC) provide environmental context only and are not simultaneous with the event. The agreement among datasets is qualitative; no co-located extraction or quantitative comparison was performed.

Table 2 Timeline of multi-source observations, 6 April 2026 (UTC)

Time (UTC)	Radar (CMAX)	Himawari-9 (BT / CCO)	AWS rainfall
06:00–06:20	Compact cell over the airport; 42 dBZ at 06:04, 45 dBZ at 06:20	Southern cluster appears at 06:10 (BT about −48 to −56 °C), intensifying to about −56 to −62 °C by 06:30; first Cb cluster south of the airport at 06:20 (CCO)	Onset at 06:10 (0.6 mm); 9.0 mm at 06:20
06:20–06:40	Slight weakening; 40 dBZ at 06:36	Cb cluster growing (06:30); core BT about −62 to −69 °C over a larger area at 06:40	Maximum: 18.6 mm at 06:30; 13.4 mm at 06:40
06:40–07:00	Reflectivity ~44 dBZ with two cells to the NW and W at 07:00	Largest, most cohesive Cb object at 06:40–06:50; peripheral warming at 06:50–07:00	3.4 mm at 06:50; event total 45.0 mm; essentially no rain afterwards

Note: ERA5 LLMT (06:00 and 07:00 UTC) and radiosonde soundings (00 and 12 UTC) are not included because they do not resolve the 06:00–07:00 UTC timeline; they provide environmental context only. Times are UTC; cell values are taken from Figs. 2–5.

The main limitations of this study are as follows. First, the integration of the datasets is qualitative: the datasets differ in sampling interval and spatial support, and no co-located extraction or quantitative comparison was made. Second, the rainfall evidence rests on a single AWS with 10-minute resolution, whose catch may be reduced at high intensities, and the spatial distribution of rainfall over Terminal 3 itself is not resolved. Third, moisture-flux convergence was not calculated, so the LLMT magnitude fields cannot show where moisture converges, and ERA5 at 0.25° cannot resolve a convective cell a few kilometers across, and the fields at 06:00–07:00 UTC may already reflect the convection. Fourth, the radiosonde soundings at 00 and 12 UTC are not simultaneous with the event, and the 12 UTC sounding was taken after it. Fifth, radar CMAX implies rain rates well below those recorded by the AWS, so it was used qualitatively, and attenuation, calibration, beam geometry, and the cone of silence were not assessed; the CCO thresholds were adopted from Himawari-8 studies without a sensitivity test, and parallax was not corrected. Sixth, the link to the ceiling failure is inferential: the failure time comes from a social-media report, no engineering assessment or official failure time was available, the structural response was not analyzed, and a climatological assessment of the rainfall intensity at the airport was not possible.

4. CONCLUSION

This study investigated the significant weather conditions associated with the ceiling failure at Terminal 3 of Soekarno-Hatta International Airport on 6 April 2026 using an integrated multi-source observational approach comprising C-Band weather radar CMAX, Himawari-9 satellite imagery, AWS observations, ERA5 Low-Level Moisture Transport (LLMT), and radiosonde soundings. The AWS recorded 45.0 mm of rainfall between 06:10 and 06:50 UTC, with a maximum of 18.6 mm in 10 minutes

at 06:30 UTC, a temperature drop of about 7.6°C, and gusts of up to 11.5 m s^{-1}. These conditions were associated with the rapid development of a compact convective system over and around the airport between 06:04 and 07:00 UTC. Radar CMAX showed maximum reflectivity of 40–45 dBZ, which implies rain rates well below those recorded by the AWS and was therefore used only qualitatively, while Himawari-9 showed cloud-top brightness temperatures of about −62 to −69°C. Cloud Convective Overlays (CCO) analysis indicated the growth and persistence of cumulonimbus clouds south of the airport during the period of maximum rainfall. ERA5 LLMT fields at 925 and 825 hPa showed enhanced low-level moisture over western Java and the western Java Sea, with a strong gradient near the airport, indicating a moist low-level environment, although ERA5 cannot resolve the individual cell. The 00 UTC sounding showed weak CAPE (109 J kg^{-1}) and moderate KI (33.5), consistent with a low-CAPE tropical environment; the 12 UTC sounding was taken after the event and was not used to characterize the pre-storm environment. The qualitative integration of these observations indicates that the event is consistent with rapidly developing convection in a moist low-level environment that produced short-duration heavy rainfall, which coincided with, and is a plausible contributing condition for, the ceiling failure. The causal link and the failure mechanism were not demonstrated and require engineering investigation.

In terms of implications for airport operations and forecasting, cold cloud tops near the airport domain were already present at 05:40 UTC and a compact radar echo was over the airport at 06:04 UTC, before rainfall onset at the AWS (06:10 UTC), which suggests that nowcasting products based on radar CMAX and Himawari CCO detection could support short-lead alerts for very heavy rainfall. Such alerts could be combined with drainage and roof-load monitoring at terminal buildings. Future work should compute moisture-flux convergence, $-\nabla\cdot(qV)$, from ERA5 or high-resolution model fields, add nearby rain gauges and dual-polarization radar quantities, ERA5 or high-resolution model fields for the hours before initiation, and a post-event structural assessment of Terminal 3.

ACKNOWLEDGMENTS

The authors would like to acknowledge the institutions and personnel responsible for providing meteorological observations and supporting data used in this study, including weather radar, automatic weather station, satellite, and atmospheric reanalysis datasets. The authors also appreciate the technical and academic support provided during the research.

AUTHOR CONTRIBUTIONS

Conceptualization, L.O.A.N. and S.A.S.; methodology, L.O.A.N. and S.A.S.; formal analysis, L.O.A.N.; investigation, L.O.A.N.; data curation, L.O.A.N.; visualization, L.O.A.N.; writing—original draft preparation, L.O.A.N.; writing—review and editing, L.O.A.N. and S.A.S.; supervision, S.A.S. All authors have read and agreed to the published version of the manuscript.

FUNDING

This research received no external funding.

DATA AVAILABILITY STATEMENT

The meteorological data analyzed in this study include weather radar observations, automatic weather station measurements, Himawari-9 satellite imagery, ERA5 reanalysis data, and radiosonde observations. Publicly available datasets can be accessed through their respective data providers, while data subject to access restrictions may be requested from the corresponding author, subject to the relevant data-sharing policies.

CONFLICTS OF INTEREST

The authors declare no conflict of interest.

ARTIFICIAL INTELLIGENCE (AI) USAGE DECLARATION

AI-assisted tools were used for language editing and editorial proofreading during manuscript preparation. The authors reviewed and verified the edited content and take full responsibility for the accuracy, originality, scientific validity, and integrity of the manuscript.

REFERENCE

Adzan, M. A., Setyowati, P. R., & Haryanto, Y. D. (2025). Analysis of significant weather phenomena triggering diversions at Soekarno-Hatta International Airport using multi-data observations (case study of January 28, 2025). *Jurnal Geografi: Geografi dan Pengajarannya, 23*(2), 303–316. https://doi.org/10.26740/jggp.v23n2.p303-316

Badan Meteorologi, Klimatologi, dan Geofisika. (2010). *Peraturan Kepala BMKG Nomor KEP.009 Tahun 2010 tentang prosedur standar operasional pelaksanaan peringatan dini, pelaporan, dan diseminasi informasi cuaca ekstrim.*

Fibriantika, E., & Mayangwulan, D. (2020). Analisis spasial indeks stabilitas udara di Indonesia [Spatial analysis of air stability index in Indonesia]. *Jurnal Sains & Teknologi Modifikasi Cuaca, 21*(1), 1–12. https://doi.org/10.29122/jstmc.v21i1.4005

Gössling, S., Neger, C., Steiger, R., & Bell, R. (2023). Weather, climate change, and transport: A review. *Natural Hazards, 118*(2), 1341–1360. https://doi.org/10.1007/s11069-023-06054-2

Hastuti, M. I., & Mulsandi, A. (2017). Pemantauan sebaran awan konvektif menggunakan metode Cloud Convective Overlays dan Red Green Blue Convective Storms pada satelit Himawari-8 (studi kasus: Hujan ekstrim Bima 21 Desember 2016). In *Prosiding Seminar Nasional Penginderaan Jauh ke-4 Tahun 2017* (pp. 477–483).

Hersbach, H., Bell, B., Berrisford, P., Hirahara, S., Horányi, A., Muñoz-Sabater, J., Nicolas, J., Peubey, C., Radu, R., Schepers, D., Simmons, A., Soci, C., Abdalla, S., Abellan, X., Balsamo, G., Bechtold, P., Biavati, G., Bidlot, J., Bonavita, M., ... Thépaut, J.-N. (2020). The ERA5 global reanalysis. *Quarterly Journal of the Royal Meteorological Society, 146*(730), 1999–2049. https://doi.org/10.1002/qj.3803

Jarošová, M., & Janošková, A. (2023). Meteorological causes of air accidents. *Transportation Research Procedia, 75*, 183–188. https://doi.org/10.1016/j.trpro.2023.12.021

Kim, K., Lee, H., Lee, M., Bae, Y. H., Kim, H. S., & Kim, S. (2023). Analysis of weather factors on aircraft cancellation using a multilayer complex network. *Entropy, 25*(8), Article 1209. https://doi.org/10.3390/e25081209

Kompas.com. (2026a, April 6). *Plafon Terminal 3 Bandara Soetta jebol akibat hujan deras, penumpang berlarian.* https://megapolitan.kompas.com/read/2026/04/06/15470091/plafon-terminal-3-bandara-soetta-jebol-akibat-hujan-deras-penumpang (Accessed on October 1, 2026).

Kompas.com. (2026b, April 8). *Plafon Terminal 3 Bandara Soetta jebol, ditargetkan selesai diperbaiki hari ini.* https://megapolitan.kompas.com/read/2026/04/08/12073101/plafon-terminal-3-bandara-soetta-jebol-ditargetkan-selesai-diperbaiki (Accessed on October 1, 2026).

Kusumawardani, N., & Azani, A. A. (2022). Kajian indeks stabilitas atmosfer terhadap kejadian hujan lebat di Kota Bitung (studi kasus tahun 2020–2021). *Jurnal Widya Climago, 4*(1).

Kwasiborska, A., Grabowski, M., Sedláčková, A. N., & Novák, A. (2023). The influence of visibility on the opportunity to perform flight operations with various categories of the instrument landing system. *Sensors, 23*(18), Article 7953. https://doi.org/10.3390/s23187953

Liu, K., Wang, Q., Wang, M., & Koks, E. E. (2023). Global transportation infrastructure exposure to the change of precipitation in a warmer world. *Nature Communications*, *14*(1), 2541. https://doi.org/10.1038/s41467-023-38203-3

Lubis, S. W., Hagos, S., Hermawan, E., Respati, M. R., Ridho, A., Risyanto, Paski, J. A. I., Muhammad, F. R., Siswanto, Ratri, D. N., Setiawan, S., & Permana, D. S. (2022). Record-breaking precipitation in Indonesia's capital of Jakarta in early January 2020 linked to the northerly surge, equatorial waves, and MJO. *Geophysical Research Letters, 49*(22), Article e2022GL101513. https://doi.org/10.1029/2022GL101513

Metro TV News. (2026, April 6). *Atap Terminal 3 Bandara Soekarno-Hatta jebol akibat hujan deras.* https://www.metrotvnews.com/read/bD2CwJXn-atap-terminal-3-bandara-soekarno-hatta-jebol-akibat-hujan-deras (Accessed on October 1, 2026).

Mulya, A. (2021). Identifikasi sebaran awan konvektif menggunakan metode RGB dan CCO pada data satelit Himawari-8 (studi kasus hujan lebat Putussibau 10 September 2020). *Jurnal Ilmiah Matematika, 8*(1), 11. https://doi.org/10.26555/konvergensi.v8i1.21457

Nisa, A. A., Sukojo, B. M., & Nurwatik, N. (2022). Analysis of weather change using Himawari-8 satellite image with 24-hours microphysics RGB and convective available potential energy method (study case: Flood Central Kalimantan 18–24 August 2021). In *2022 IEEE Asia-Pacific Conference on Geoscience, Electronics and Remote Sensing Technology (AGERS)* (pp. 146–151). IEEE. https://doi.org/10.1109/AGERS56232.2022.10093664

Paski, J. A. I., Alfahmi, F., Permana, D. S., & Makmur, E. E. S. (2020). Reconstruction of extreme rainfall event on September 19–20, 2017, using a weather radar in Bengkulu of Sumatra Island. *The Scientific World Journal, 2020*, Article 1639054. https://doi.org/10.1155/2020/1639054

Pauley, P. M., & Ingleby, B. (2022). Assimilation of in-situ observations. In S. K. Park & L. Xu (Eds.), *Data assimilation for atmospheric, oceanic and hydrologic applications* (Vol. IV, pp. 293–371). Springer. https://doi.org/10.1007/978-3-030-77722-7_12

Saputra, A. I., & Darmawan, Y. (2025). Analisis hujan ekstrem menggunakan data satelit Himawari 9, model, dan observasi (studi kasus: Jakarta Utara, 29 Februari 2024). *Jurnal Penelitian Fisika dan Terapannya (JUPITER), 6*(2), 9–21. https://doi.org/10.31851/jupiter.v6i2.17976

Sasmito, A., Permana, D. S., Praja, A. S., & Haryoko, U. (2020). Pengaruh microburst dan low-level wind shear (LLWS) pada kasus kecelakaan pendaratan pesawat Lion Air tanggal 13 April 2013 di Bali. *Jurnal Meteorologi dan Geofisika, 21*(1), 1–8. https://doi.org/10.31172/jmg.v21i1.549

Sokol, Z., Szturc, J., Orellana-Alvear, J., Popová, J., Jurczyk, A., & Célleri, R. (2021). The role of weather radar in rainfall estimation and its application in meteorological and hydrological modelling—A review. *Remote Sensing, 13*(3), Article 351. https://doi.org/10.3390/rs13030351

Suara.com. (2026, April 6). *Bandara Soetta hujan ekstrem, atap Terminal 3 jebol hingga 12 penerbangan gagal mendarat.* https://www.suara.com/bisnis/2026/04/06/180945/bandara-soetta-hujan-ekstrem-atap-terminal-3-jebol-hingga-12-penerbangan-gagal-mendarat

Syaifullah, M. D. (2017). Analisis kondisi udara atas wilayah Indonesia dengan data radiosonde. *Jurnal Meteorologi dan Geofisika, 18*(1). https://doi.org/10.31172/jmg.v18i1.268

Syaifullah, M. D., & Nuryanto, S. (2016). Pemanfaatan data satelit GMS multi kanal untuk kegiatan teknologi modifikasi cuaca. *Jurnal Sains & Teknologi Modifikasi Cuaca, 17*(2), 47–55. https://doi.org/10.29122/jstmc.v17i2.525

Taszarek, M., Allen, J. T., Marchio, M., & Brooks, H. E. (2021). Global climatology and trends in convective environments from ERA5 and rawinsonde data. *npj Climate and Atmospheric Science, 4*(1), Article 35. https://doi.org/10.1038/s41612-021-00190-x

Tondang, Y. M., Situmorang, M., Ikhsan, T., & Darmawan, Y. (2023). Accuracy of weather radar products for rainfall estimation in North Sumatra region. *Prisma Sains: Jurnal Pengkajian Ilmu dan Pembelajaran Matematika dan IPA IKIP Mataram, 11*(2), 351–357. https://doi.org/10.33394/jps.v11i2.7720

Txt Transportasi Umum. (2026, April 6). *[Post on X].* X. https://x.com/txttransportasi/status/2041094978961854882